Journal of The Electrochemical Society

The Electrochemical Society
Advancing solid state & electrochemical science & technology

RESEARCH PAPER • OPEN ACCESS

Facile Surface Coatings for Performance Improvement of NMC811 Battery Cathode Material

To cite this article: Xiao-Guang Sun *et al* 2022 *J. Electrochem. Soc.* **169** 020565

View the article online for updates and enhancements.

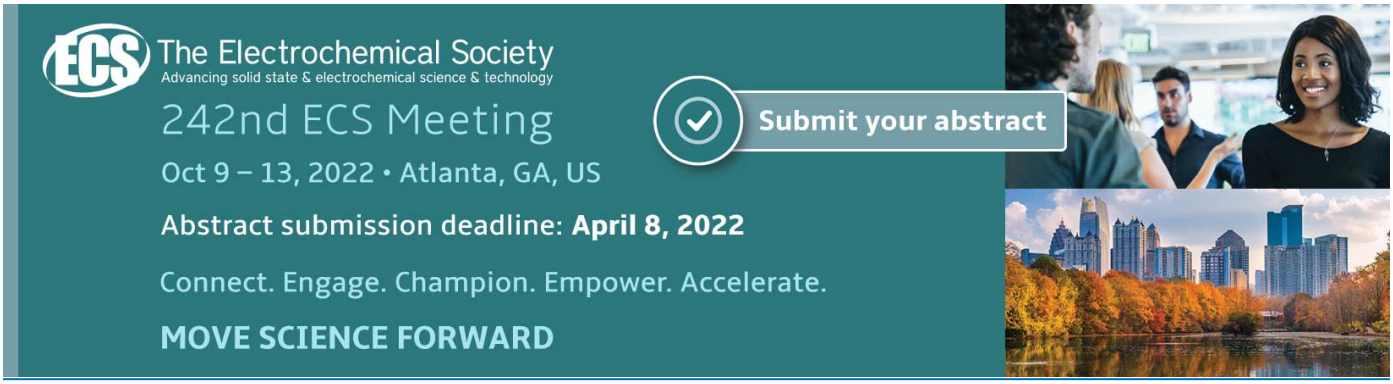

This content was downloaded from IP address 192.31.96.218 on 02/03/2022 at 16:02

Journal of The Electrochemical Society, 2022 **169** 020565

Facile Surface Coatings for Performance Improvement of NMC811 Battery Cathode Material

Xiao-Guang Sun,[1,z] Charl J. Jafta,[2] Susheng Tan,[3] Albina Borisevich,[4] Ram B. Gupta,[5] and Mariappan Parans Paranthaman[1,*,z]

[1]*Chemical Sciences Division, Oak Ridge National Laboratory, Oak Ridge, Tennessee 37831, United States of America*
[2]*Electrification and Energy Infrastructure Division, Oak Ridge National Laboratory, Oak Ridge, Tennessee 37831, United States of America*
[3]*Department of Electrical and Computer Engineering, and Petersen Institute of NanoScience and Engineering, University of Pittsburgh, Pittsburgh, Pennsylvania 15261, United States of America*
[4]*Center for Nanophase Materials Sciences, Oak Ridge National Laboratory, Oak Ridge, Tennessee 37831, United States of America*
[5]*Department of Chemical and Life Science Engineering, Virginia Commonwealth University, Richmond, Virginia 23284, United States of America*

High nickel content layered oxide $LiNi_{0.8}Mn_{0.1}Co_{0.1}O_2$ (NMC811) is a promising cathode material with a high theoretical capacity of 200 mAh g^{-1} for use in high energy density lithium-ion batteries. However, its surface can easily get passivated by LiOH and Li_2CO_3 due to its surface residual Li_2O being reacting with ambient moisture and CO_2. Herein, NMC811 was treated in a 3.0 M solution of lithium bis(fluorosulfonyl)imide (LiFSI) in dimethyl carbonate (DMC) at 60 °C for 8 h, 16 h and 24 h, respectively, resulting in coating of the NMC811 surface with LiF due to the basic nature of those residual lithium salts that react with LiFSI. The facile treatment of NMC811 in LiFSI/DMC not only improves the cycling stability but also enhances the capacity of the Li/NMC811 cells, mainly because of the thinning of the Li_2CO_3 layer as suggested by cyclic voltammograms and impedance analyses. This method opens a new avenue for activation of passivated NMC811 particles for practical battery applications.
© 2022 The Electrochemical Society ("ECS"). Published on behalf of ECS by IOP Publishing Limited. This is an open access article distributed under the terms of the Creative Commons Attribution 4.0 License (CC BY, http://creativecommons.org/licenses/by/4.0/), which permits unrestricted reuse of the work in any medium, provided the original work is properly cited. [DOI: 10.1149/1945-7111/ac5302]

Manuscript submitted December 15, 2021; revised manuscript received February 1, 2022. Published February 23, 2022.

Among various cathode materials for high energy density lithium-ion batteries (LIBs), Ni-rich lithium nickel cobalt manganese oxides such as $LiNi_{0.6}Mn_{0.2}Co_{0.2}O_2$ (NMC622) and $LiNi_{0.8}Mn_{0.1}Co_{0.1}O_2$ (NMC811) have been intensively investigated due to their high capacity and low cost.[1–6] Particularly, the latter NMC811, which can reach a high specific capacity of ~200 mAh g^{-1} with an upper cut-off voltage of 4.3 V vs Li/Li^+, is a very promising high voltage cathode material for LIBs. Unfortunately, poor cycling stability was usually observed for the NMC based LIBs due to electrolyte oxidation at the cathode surface and structural changes of the materials at high potentials or high temperatures.[7–10] It has been reported that Ni-rich cathode materials with a layered structure could easily change from the layered phase ($R\bar{3}m$) to the spinel-like phase ($Fd\bar{3}m$) and rock-salt phase ($Fm\bar{3}m$) during high voltage cycling and at high temperatures.[8,11–15] In the surface structure change, part of lithium and oxygen ions were lost from the NMC cathode surface due to transition metal ions (Ni^{2+}) migrating to the lithium ions sites, resulting in capacity loss and cell impedance increase[16,17] So far, various methods such as electrolyte additives,[18–21] surface coating,[11,14,22–32] doping,[23,31–35] as well as core–shell structure design,[16,36] have been adopted to improve the cycling stability of NMC or related layer cathode materials. The essence of surface coating is to either remove residual lithium compounds or prevent the surface reactive sites from initiating parasitic reactions, which can thus improve coulombic efficiency and cycling stability.[15,23,24,37,38]

Recently, Zhang et al. reported a facile coating process using $LiPF_6$ as a cathode additive, which was accomplished by ball milling an NMC-$LiPF_6$-N-methyl pyrrolidinone (NMP) suspension.[38] The milling process resulted in NMC surface being coated with a mixture of Li_3PO_4-LiF, which not only improved the cycling stability but also enhanced the rate capability of the Li/NMC811 cells.[38] The surface coating of Li_3PO_4-LiF is dominated by the thermodynamic stable LiF, which is evidenced by the stability of the solid electrolyte interphases (SEIs) and the cycling performance. Inspired by this simple and practically feasible process, we are exploring alternative precursors that can also generate LiF dominant SEIs. In 2018, Ishikawa et al. reported that LiF was observed at the surface of graphite electrodes taken out from a solution of 2.00 mol kg^{-1} lithium bis(fluorosulfonyl)imide (LiFSI) in 1-ethyl-3-methylimidazolium (EMIm.FSI) and from 0.32 mol kg^{-1} LiFSI/EMImFSI system with pre-heat treatment at 50 °C before the initial lithiation process.[39] They claimed that the observed LiF formation on the surface of graphite electrode was not due to a massive thermal decomposition or hydrolysis of FSI because LiFSI was shown to be stable well above 100 °C even in the presence of 6 wt.% H_2O,[40] and therefore graphite electrode played an important role in the decomposition of FSI anions.[39] Similarly, we have also observed LiF formation at the open cell voltage of a hard carbon half-cell in 0.5 M LiFSI/EMIm.FSI ionic liquid electrolyte.[41] The easy formation of LiF in FSI based ionic liquid electrolyte prompted us to investigate LiFSI based solutions for treatment of NMC cathode materials and its effect on cycling performance of the cathode materials. However, rather than using ionic liquids solutions, we will use simple organic solvent-based LiFSI solutions as it is the LiFSI salt, not the ionic liquids, that contributes to the formation of LiF, unlike in the Li metal batteries with an imidazolium ionic liquid electrolyte where the potential formation of carbenes from the imidazolium cation can trigger the decomposition of the FSI anions as illustrated in our previous investigation.[41]

Experimental

Materials.—NMC811 was purchased from Targray and treated at 120 °C for overnight before use. N-methyl-pyrrolidone (NMP) was purchase from Aldrich and used as received. Polyvinylidene fluoride (PVdF) and C45 were purchased from MTI Corporation. LiFSI was purchased from Oakwood Chemical and dried at 80 °C under high vacuum for 48 h before use. A solution of 3.0 mol kg^{-1} LiFSI in dimethyl carbonate (DMC) was prepared in an Ar filled glove box by adding an appropriate amount of lithium bis(fluorosulfonyl)imide (LiFSI) in DMC. For the treatment procedure of NMC811, typically,

*Electrochemical Society Member.
[z]E-mail: sunx@ornl.gov; paranthamanm@ornl.gov

2.0 g of NMC811 was suspended in 2.0 g of 3.0 M LiFSI/DMC solution and stirred at 60 °C for 8 h, 16 h and 24 h, respectively. The suspensions were then filtered and washed with anhydrous DMC for three times, followed by drying at 110 °C for overnight under vacuum before casting electrode.

Electrochemistry.—NMC811 electrode was prepared by mixing the NMC811 powder with C45 (carbon black: CB) and PVdF in NMP in a 90:5:5 (NMC811:CB:PVdF) ratio to form a well homogenized slurry, which was then cast onto Al foil by the doctor blade method and left under a UV light to allow the solvent (NMP) to evaporate. The electrode was then dried in a vacuum oven overnight at 110 °C. The electrode was cut into circular discs with an area of 1.27 cm^2 and transferred to an Ar filled glove box. The electrodes have an active material loading of approximately 3–4 mg cm^{-2}. Li/NMC811 cells were assembled with Celgard 2320 as the separator and 1.2 M $LiPF_6$ dissolved in a mixture of ethylene carbonate (EC) and ethyl methyl carbonate (EMC) at a weight ratio of 3:7 as the electrolyte inside an Ar filled glovebox with the oxygen and water levels below 0.5 ppm.

Li/NMC811 cells were first formed at a current rate of C/10 for two cycles, followed by cycling at C/2 between the voltage range of 3.0 and 4.3 V. Cyclic voltammograms (CVs) were recorded on a Biologic VSP instrument in the voltage range of 3.0–4.5 V at a scan rate of 0.05 mV s^{-1}. Electrochemical impedance spectra (EIS) were tested on the same instrument with AC signal amplitude of 10 mV in the frequency range from 200 kHz to 10 mHz. For the combined CV-EIS experiment, a sequence of CV, 30 min rest, EIS was used for six cycles.

Characterization.—The XPS data were obtained by using an Al K_α X-ray source operated at 15 kV for an applied power of 300 W. Charge correction was done by shifting all the peaks relative to the C-C peak at a binding energy of 284.8 eV. All the XPS spectra were fitted using CasaXPS. Annular bright field (ABF) scanning transmission electron microscopy (STEM) data were recorded using Nion UltraSTEM 200 microscope operated at 200 kV. Lattice spacings were measured using image diffractograms. Scanning Electron Microscopy (SEM) images were acquired using Hitachi S-4800 SEM operated at 5 kV.

Results and Discussion

The driving force for LiF formation by treatment of NMC811 in 3.0 M LiFSI/DMC solution at 60 °C is the presence of alkaline species such as Li_2O, LiOH and Li_2CO_3, of which the latter two species (LiOH and Li_2CO_3) are derivatives from the first one (Li_2O) reacting with moisture and CO_2 in air.[26,42] In the presence of the above basic species and heating at 60 °C, the weak S-F bonds of LiFSI can be easily broken and form LiF via the following routes:[41]

$$Li(NSO_2F)_2 + Li_2O \rightarrow Li(FSO_2NSO_3Li) + LiF \quad [1]$$

$$Li(NSO_2F)_2 + 2LiOH \rightarrow Li(FSO_2NSO_3Li) + LiF + H_2O \quad [2]$$

$$Li(NSO_2F)_2 + Li_2CO_3 \rightarrow Li(FSO_2NSO_3Li) + LiF + CO_2 \quad [3]$$

$$Li(FSO_2NSO_3Li) + Li_2O \rightarrow Li(NSO_3Li)_2 + LiF \quad [4]$$

$$Li(FSO_2NSO_3Li) + 2LiOH \rightarrow Li(NSO_3Li)_2 + LiF + H_2O \quad [5]$$

$$Li(FSO_2NSO_3Li) + Li_2CO_3 \rightarrow Li(NSO_3Li)_2 + LiF + CO_2 \quad [6]$$

Figure 1 shows the X-ray powder diffraction (XRD) patterns of the pristine and 24 h treated NMC811 samples. No impurities are detected in the treated sample as compared to the pristine sample, indicating that the treatment in LiFSI/DMC doesn't alter the bulk structure of the materials. However, if looked carefully, two minor changes can still be identified. First, the ratio of the two major peaks at 003 and 104 (*I003/I104*), which has been indirectly related to the cation mixing between Li^+ and Ni^{2+} in the lithium layer,[13,43–46] increases from 1.47 for the baseline material to 1.54 for the 24 h treated sample. Second, there is a clear shift of the (003) peak of the 24 h treated sample towards lower angle (zoomed-in spectra of Fig. 1). This shift implies that the crystal cell along the c direction is enlarged, which can enhance the kinetics of Li^+ during cycling.

To check the effect of treatment on the morphologies of NMC811 materials, imaging using SEM and high resolution ABF STEM were carried out. As shown in Fig. 2, the sphere like morphology from aggregations of the primary particles does not change after treatment for 24 h (Figs. 2c and 2d vs Figs. 2a and 2b). The surface features on the NMC811 particles can be observed in the ABF STEM images (Figs. 2f and 2h). In addition, the lattice spacing, which corresponds to (003) planes from the rhombohedral phase, increases from 4.7 Å for the pristine sample to 4.9 Å for the 24 h treated sample. which is consistent with the observed (003) peak shift in XRD (Fig. 1).

The baseline and treated NMC811 powders were further characterized by X-ray photoelectron spectroscopy (XPS). Figure 3a shows the C 1s spectra of the baseline and treated NMC811 samples. Besides the adventitious carbon species at 284.8 eV,[41] a dominant carbonate peak at 290 eV is observed in all samples, which can be attributed to the surface Li_2O species reacting with CO_2 in the air.[26,42] Although the proposed reaction routes 3 and 6 can reduce the amount of Li_2CO_3, it is not expected in a dramatic way to reduce its apparent amount, as the reaction happens in the two-phase solid-solution interphases, not a homogeneous reaction.[38] However, it is noted in Fig. 3b that a huge LiF peak at 685 eV is observed for all the treated NMC samples. This result confirms that the above proposed reaction routes are indeed happened, leading to LiF precipitated on the surface of the NMC samples. Also, there are some minor FSI segment related species observed at 687.8 and 688.8 eV, respectively.[47,48] Similarly, two N 1s species related to FSI anion are identified at 398.7 and 400 eV, respectively. The aforementioned minor F 1s species are closely related to the N 1s species, which can be assigned to the some residual LiFSI and its partial decomposition product of $Li(FSO_2NSO_3Li)$ as proposed in routes 1–3, respectively.[47] Figures 3d–3g show the Li 1s spectra of the pristine and treated NMC811 samples. Clearly, besides the dominant Li_2CO_3 peaks, LiF can be observed for the three treated samples. In addition, due to the dominance of Li_2CO_3, it is hard to identify other LiFSI decomposition species such as $Li(FSO_2NSO_3Li)$ and $Li(NSO_3Li)_2$. On one hand, these XPS results confirm that LiF indeed precipitated on the surface of the NMC cathode powders during the heat treatment in 3.0 M LiFSI/DMC solutions. On the other hand, it seems that the length of treatment time does not result in too much difference of LiF coverage on the surface. However, from the point of slow reaction kinetics of two-phase solid-solution reactions, Li_2CO_3 should decrease while LiF increases with treatment time at 60 °C, as suggested by the following electrochemical impedance spectroscopy (EIS) measurement.

The effect of surface treatment on the NMC cathode materials was characterized by first cycling under a low current rate of C/10 for two cycles, followed by cycling at a constant current rate of C/2 between the voltage range of 3.0 and 4.5 V. Three cells for each samples were assembled and evaluated and Fig. 4a summaries the averaged results with error bars. Several apparent trends can be observed from Fig. 4a. First, both the pristine and treated samples show initial gradual increase of capacity, followed by gradual decrease. Second, it takes more cycles for the pristine sample to reach the maximum capacity than those of the treated samples. Third, 24 h sample has the highest capacity among all the four samples. These features are closely related to the observed strong Li_2CO_3 peaks in all the samples, which result in high polarizations in all the samples as observed in Fig. 4b during the first charge (i.e., delithiation) process, leading to the initial charge voltage overshoot above 4.0 V (inset of Fig. 4b). In addition, the surface Li_2CO_3 layer not only results in high polarization but also leads to low capacities.

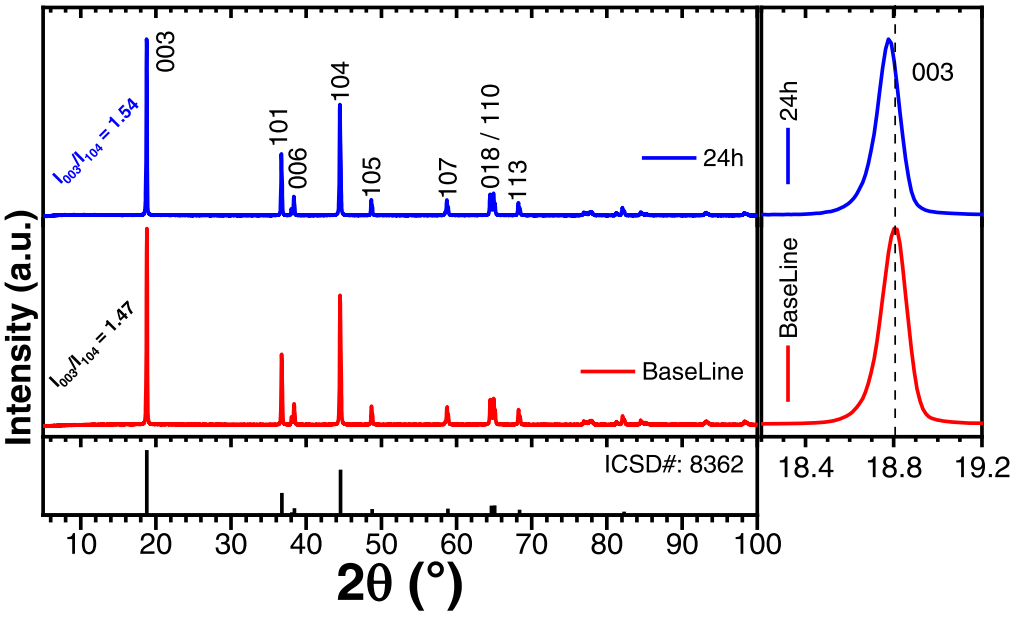

Figure 1. XRD patterns of pristine and 24 h treated NMC811 samples.

As shown in Fig. 4b, the initial discharge (lithiation)/charge (delithiation) capacities are 85.0, 109.6, 107.5, 109.7, and 110.2, 139.4, 137.8, 140.0 mAh g^{-1} for the pristine, 8 h, 16 h, and 24 h NMC sample, respectively, resulting in initial coulombic efficiencies of 77.1%, 78.6%, 78.0%, and 78.4%. For the second cycle (Fig. 4c), the corresponding discharge/charge capacities increase to 104.9, 124.7, 126.2, 129.0, and 108.3, 126.8, 128.8, 131.3 mAh g^{-1}, respectively, leading to increased coulombic efficiencies of 96.9%, 98.3%, 98.0%, and 98.2%. These capacities are much lower than the theoretical capacity of NMC811 (200 mAh g^{-1}) even under a low current rate of C/10, which could be ascribed to both thick Li_2CO_3 layer and high *I003/I104* ratios (Fig. 1).[46] The reversible capacities decrease to much lower values when the current increases to C/2, which gradually increase first and then decrease with cycling, as shown in both Fig. 4a. Interestingly, if the current rate is increased gradually from C/10 to C/5 and C/2, the reversible capacities increase rather than decrease (Fig. 4d). The reversible capacities only decrease when the current rate is higher than 1C (up to 5C), as normally would be observed due to the limitations of ion diffusion in both liquid electrolyte and cathode materials. However, once the current rate is reduced to C/10, much higher reversible capacities are obtained, which is consistent with the initial gradual capacity increase in Fig. 4a. It is generally recognized that the increase of capacity with cycling is due to the activation of the cathode materials, which is related to the removal of surface Li_2CO_3 species via the following routes because of the presence of trace moisture in the liquid electrolyte:[49–52]

$$LiPF_6 \rightleftharpoons LiF + PF_5 \quad [7]$$

$$PF_5 + H_2O \rightarrow PO_3F + 2HF \quad [8]$$

$$LiPF_6 + H_2O \leftrightarrow POF_3 + 2HF + LiF \quad [9]$$

$$2Li_2CO_3 + 2HF \rightarrow 2LiF + H_2O + 2CO_2 \quad [10]$$

To better understand the initial increase of capacity with cycling, cyclic voltammograms (CV) and EIS were carried out for six cycles. A 30 min rest was set between the measurements of CV and EIS, and the results are shown in Fig. 5. Overall, four distinct oxidation peak at 3.71 V, 3.78 V, 4.01 V, and 4.22 V are observed during the delithiation process, which are corresponding to the multiphase transitions of hexagonal to monoclinic (H1/M), monoclinic to hexagonal (M/H2), and hexagonal to hexagonal (H2/H3).[46] The corresponding reduction peaks are observed at 3.72 V, 3.99 V, and 4.17 V, with the first peak representing two peaks being merged as one. Comparing the CV of the pristine NMC sample with those of the treated ones, it appears that there is an apparent peak separation between H1 + M and M as marked in Fig. 4e with increasing treatment time, particularly during the second cycle. It is more interesting to compare the EIS of the pristine sample and those of the treated ones, which all exhibit strongly superimposed semi-cycle at the high frequency and medium frequency and a sloping at low frequency ranges. The intercept at the high frequency is the bulk resistance (R_b) mainly related to the ionic conductivity of the electrolyte, the semicircle at high frequency is related to the resistance of the surface layer (R_{SEI}) and the semicircle at medium frequencies is the Faradic charge-transfer resistance (R_{ct}), whereas the slope at low frequency is the Warburg impedance arising from the semi-infinite diffusion of lithium ion in the solid electrodes.[53] To get values of R_{SEI} and R_{ct}, an equivalent circuit shown in Fig. 6, where C_{SEI} and C_{dl} are capacitances of the SEI film and double-layer, respectively, has been used to fit the EIS data in Fig. 5. The obtained data of R_b, R_{SEI} and R_{ct} have been plotted in Fig. 6. The overall EIS decreasing ($R_{SEI} + R_{ct}$) with cycling is consistent with the initial increase of capacity with cycling in Fig. 4a. However, there are some big differences between the pristine sample and those treated ones, particularly the 24 h treated sample, which can only be ascribed to the treatment of the cathode samples, based on the consideration that all the cells were assembled using the same lithium ribbon with both sides being scratched. The first big difference is the much smaller R_{ct} (32 Ω) for the 24 h treated sample as compared to more than 75 Ω for the pristine and both 8 h and 16 h treated samples, which is consistent with the higher capacities and better rate capabilities for the former observed in Figs. 4a and 4d. R_{ct} for the 24 h treated sample further decreases to lower than 5 Ω after two cycles, while those of the other three samples decrease to around 20 Ω. Another big difference observed in Fig. 6 is the trend of R_{SEI}, that is, it gradually decreases for the pristine sample, while those of the treated samples, particularly the 24 h treated one increases initially then gradually decrease. The difference in R_{SEI} can be explained by two concurrent competing processes at the cathode, i.e. electrolyte oxidation and surface Li_2CO_3 reduction via the proposed routes 7–10.[49–52] For the pristine sample, Li_2CO_3 reduction is so dominant, because of its thick Li_2CO_3 layer, that R_{SEI} from Li_2CO_3 reduction is much bigger than the fresh SEI formation from

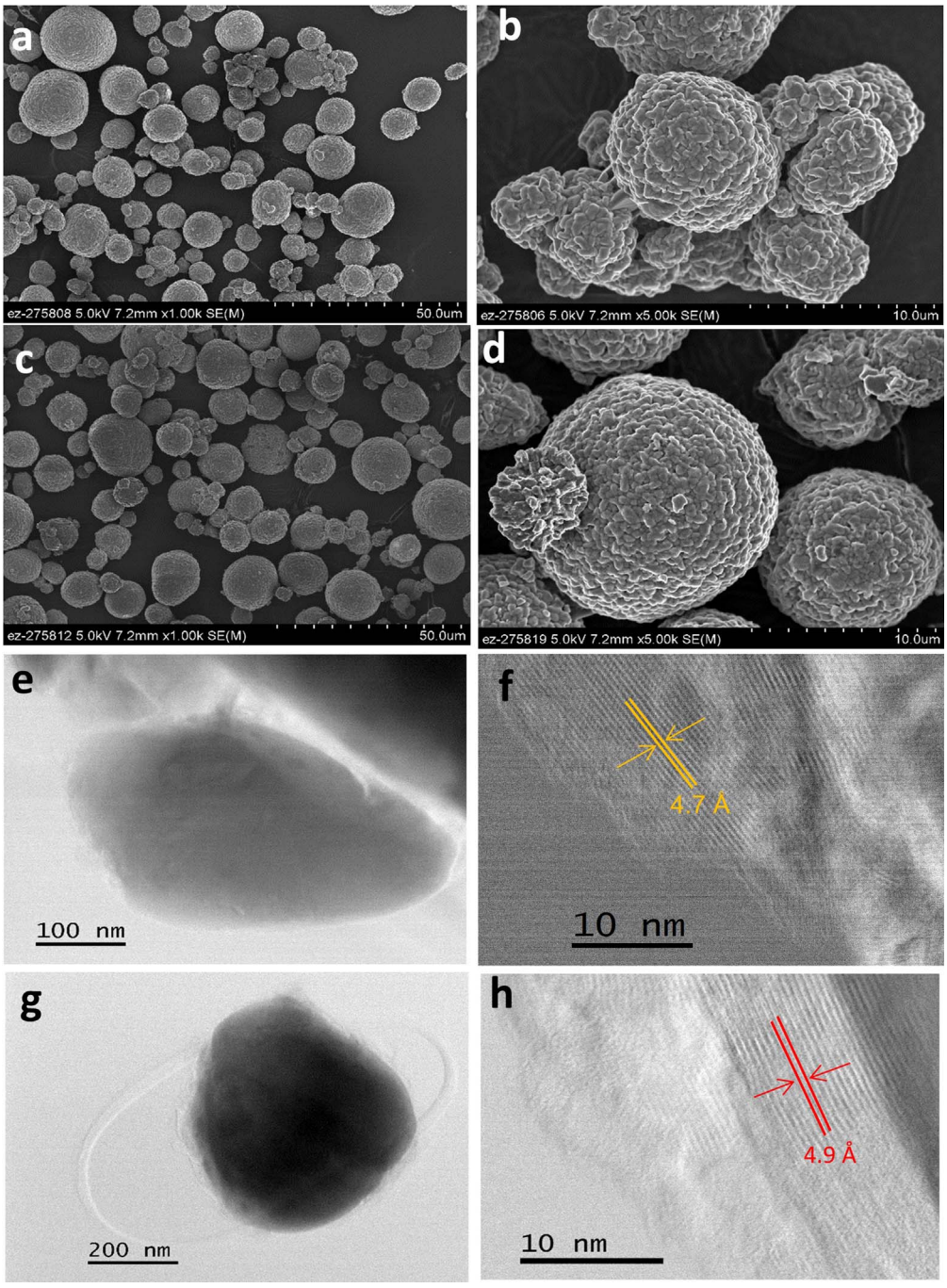

Figure 2. SEM (a)–(d) and ABF STEM (e)–(h) of the pristine (a), (b), (e) and (f) and 24 h treated (c), (d), (g) and (h) NMC811 samples.

electrolyte oxidation, resulting in overall R_{SEI} decrease with cycling. As a comparison, due to the treatment of NMC powders in LiFSI/DMC solution via reaction routes 1–6, the surface of the NMC samples have been modified, leaving more sites accessible to the electrolytes for oxidation decomposition during the initial cycles. Thus, R_{SEI} from electrolyte oxidation is bigger than that from Li_2CO_3 reduction, resulting in initial R_{SEI} increase with cycling, particularly for the 24 h sample. After the first few formation cycles, R_{SEI} from electrolyte oxidation significantly decreases while the Li_2CO_3 reduction via reactions of 7–10 continues, leading to gradual decrease of R_{SEI} with cycling. The beneficial effect of surface treatment is further confirmed by the comparison of EIS before and after cycling for the pristine and 24 h treated sample. As shown in Figs. 6e and 6f, the total EIS of the pristine sample decreases from 366 Ω before cycling to 88 Ω after 300 cycles, whereas that of the 24 h treated sample decreases from 245 Ω before cycling to 73 Ω after 300 cycles. The above results suggest that treatment of NMC powders in LiFSI/DMC provide an alternative method to activate passivated NMC and other cathode materials for application in rechargeable LIBs.

Conclusions

In summary, we have demonstrated a novel approach to activate passivated NMC811 particles via treatment in a 3.0 M LiFSI/DMC solution at 60 °C for their practical application in rechargeable LIBs. The simple treatment results in the NMC811 surface being coated with LiF, as evidenced by XPS spectra of F 1s and Li 1s, due to the basic nature of the residual lithium salts that will react with LiFSI. It has been shown that the longer treatment (24 h) can significantly

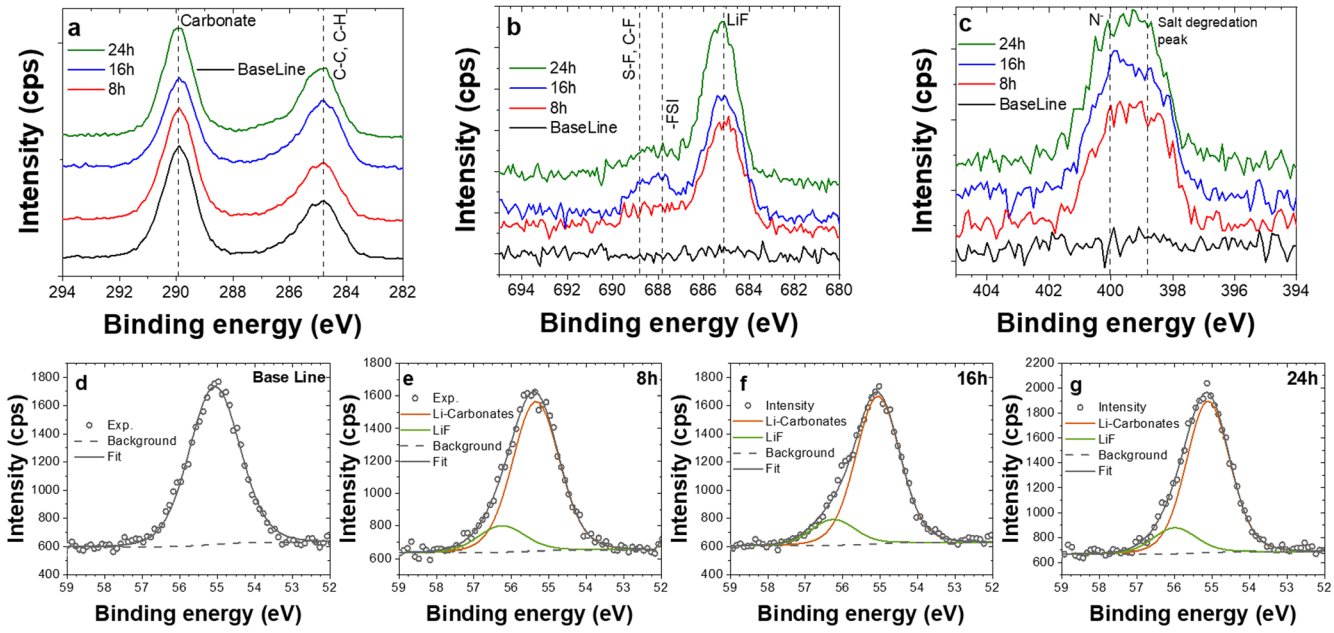

Figure 3. XPS spectra of baseline and treated NMC811 powders: (a) C 1s, (b) F 1s, (c) N 1s, and (d)–(g) Li 1s.

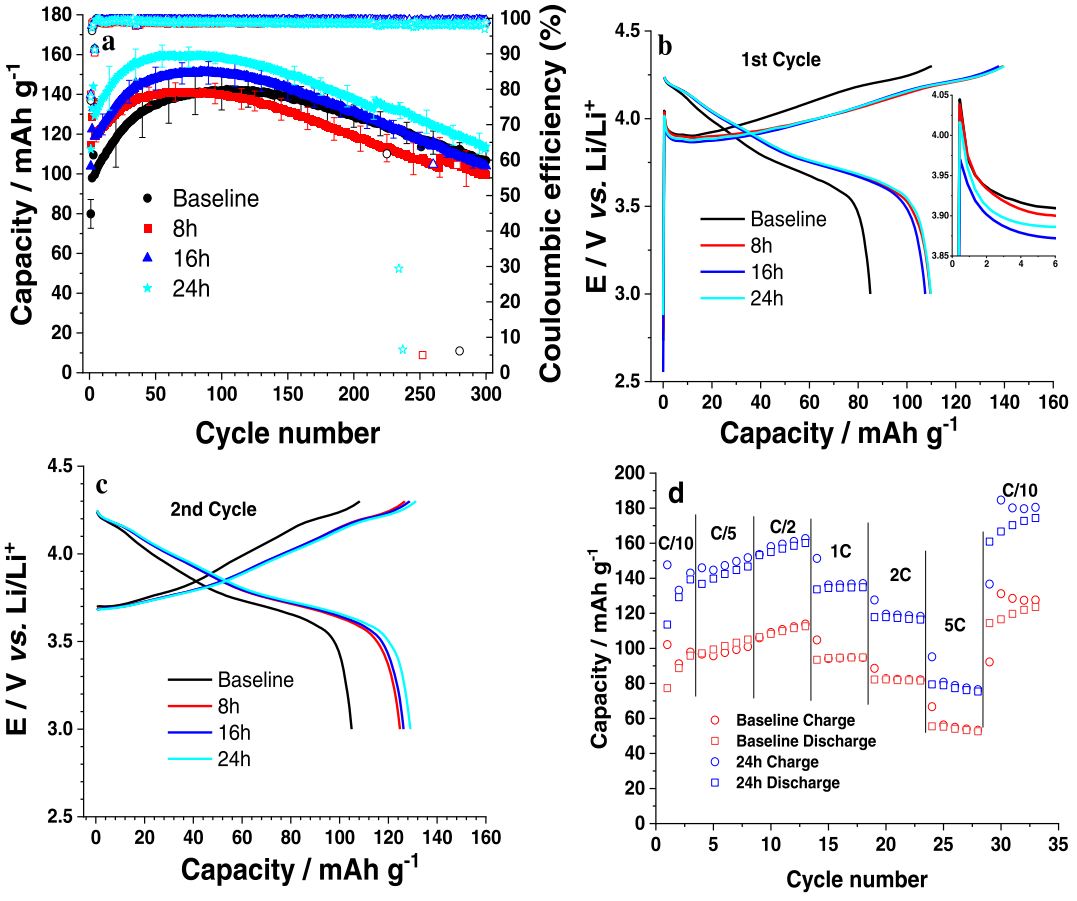

Figure 4. (a) Charge/discharge capacities of baseline and treated NMC811 samples (3 cells of each sample), (b) charge/discharge capacities and coulombic efficiencies of baseline and treated NMC811 samples with averages over three cells; Charge/discharge profiles, (c) first cycle, and (d) second cycle of the pristine and treated NMC samples at a current rate of C/10.

reduce the charge transfer resistance, leading to not only increased reversible capacity and cycling stability but also better rate capability. The results of this work indicate that heat treatment of NMC particles in LiFSI/DMC is a simple method for improving the

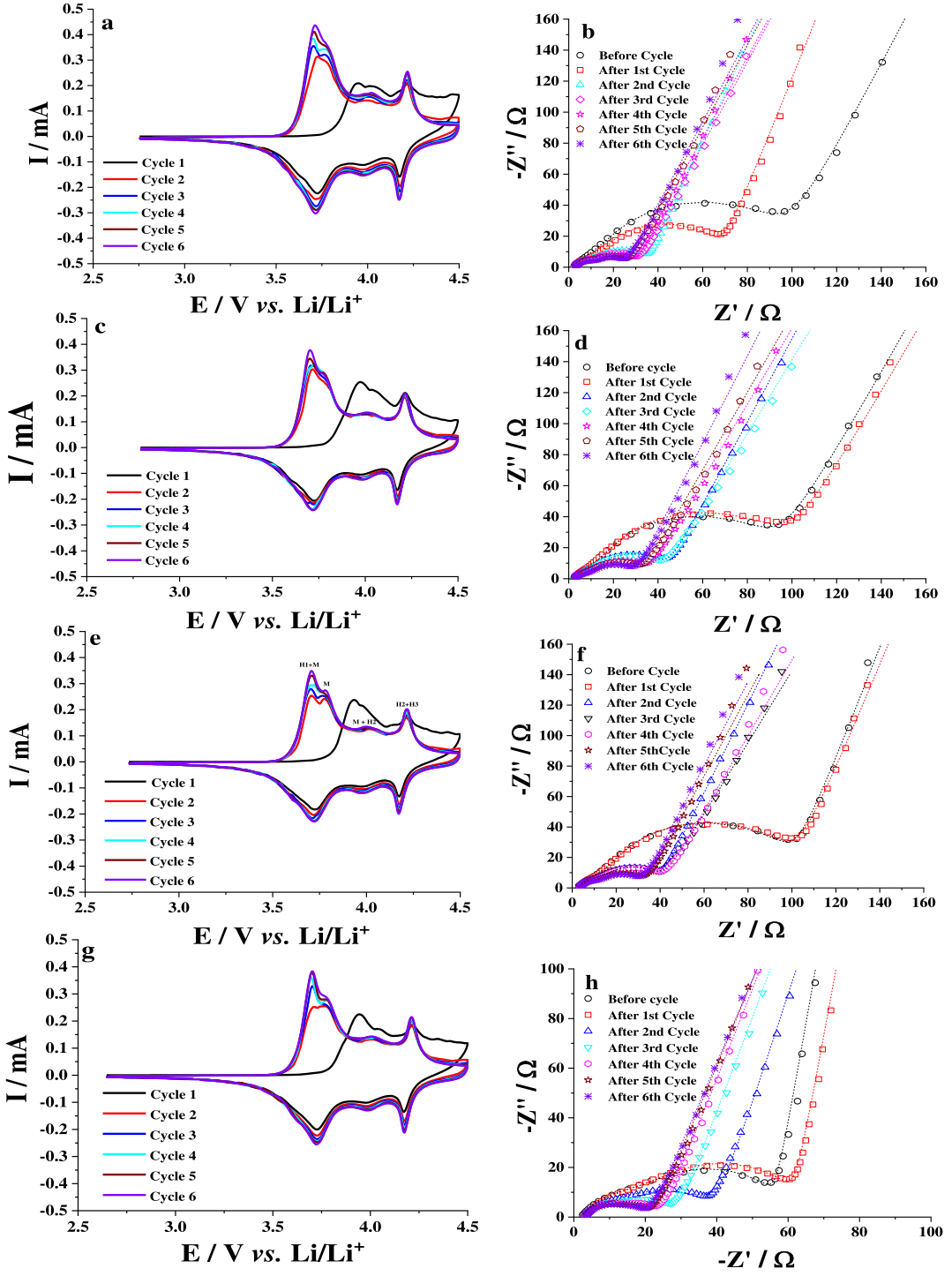

Figure 5. Cyclic voltammograms at a scan rate of 0.05 mV s^{-1} in the voltage range of 3.0−4.5 V (a), (c), (e), (g) and electrochemical impedance spectroscopy (b), (d), (f), (h) of pristine (a), (b) and treated NMC811 samples (8 h (c), (d), 16 h (e), (f) and 24 h (g), (h)).

electrochemical performance of NMC and other layered cathode materials.

Acknowledgments

All authors would like to dedicate this research to the Nobel prize winner Professor Goodenough for his 100th birthday celebration. This research was supported by the U.S. Department of Energy, Office of Energy Efficiency and Renewable Energy, Advanced Manufacturing Office. Authors gratefully acknowledge research funding from the U.S. Department of Energy via award DE-EE0009110. A.B. (electron microscopy study) was supported by the U.S. Department of Energy, Office of Science, Office of Basic Energy Sciences, Materials Sciences and Engineering Division under contract number DE-AC05-00OR22725. This manuscript has been authored by UT-Battelle, LLC under Contract No. DE-AC05-00OR22725 with the U.S. Department of Energy. The United States Government retains and the publisher, by accepting the article for publication, acknowledges that the United States Government

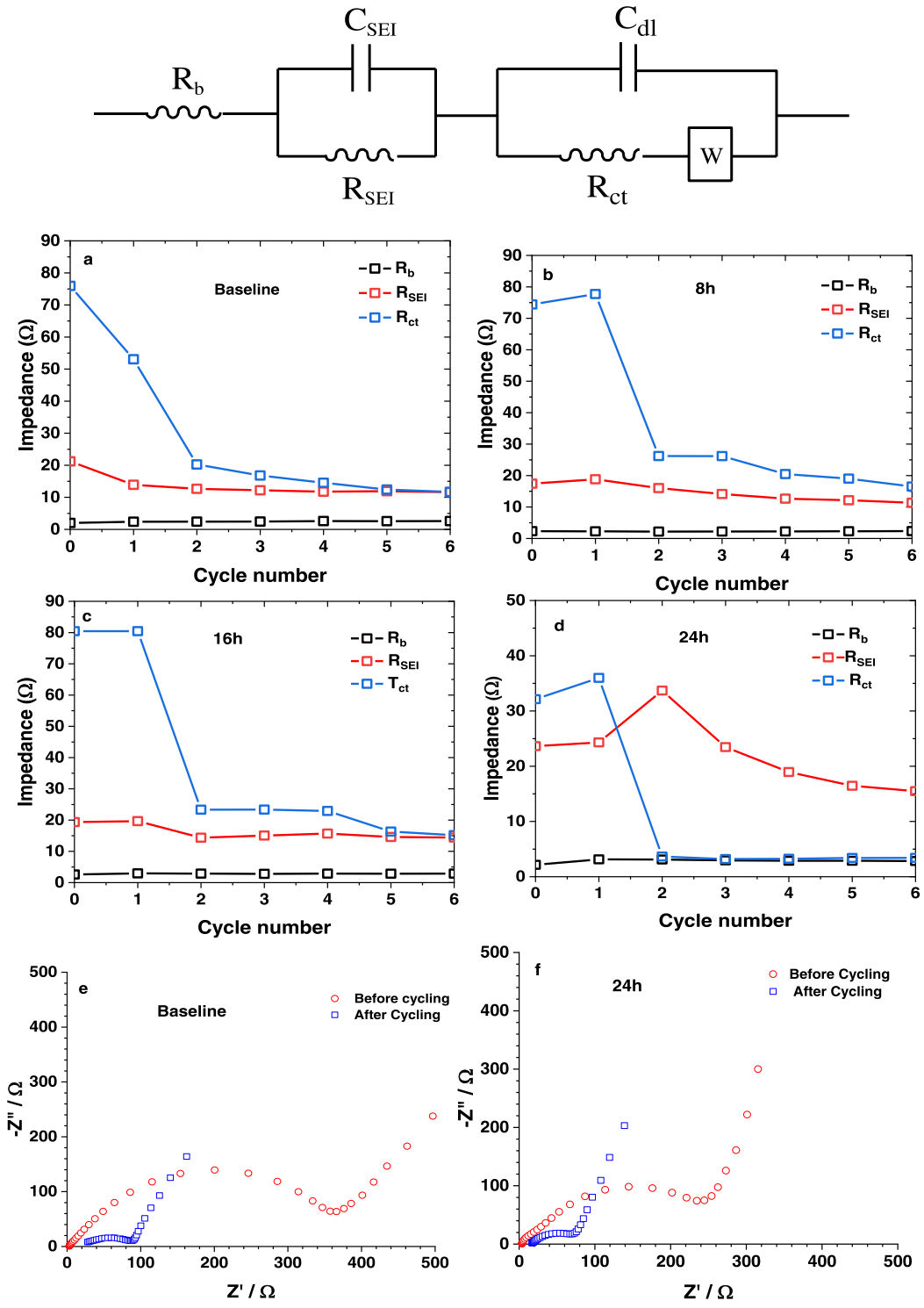

Figure 6. Equivalent circuit used to analyze the impedance spectra and the fitted EIS data of R_b, R_{SEI}, and R_{ct} for baseline (a) and treated NMC811 samples ((b) 8 h, (c)) 16 h and (d)) 24 h) from Fig. 5; EIS of the half-cells based on baseline (e) and 24 h treated (f) NMC811 samples before and after 300 cycles.

retains a non-exclusive, paid-up, irrevocable, world-wide license to publish or reproduce the published form of this manuscript, or allow others to do so, for United States Government purposes. The Department of Energy will provide public access to these results of federally sponsored research in accordance with the DOE Public Access Plan (http://energy.gov/downloads/doe-public-access-plan).

ORCID

Xiao-Guang Sun https://orcid.org/0000-0001-8451-3011
Charl J. Jafta https://orcid.org/0000-0002-9773-6799
Susheng Tan https://orcid.org/0000-0002-6162-7443
Albina Borisevich https://orcid.org/0000-0002-3953-8460
Ram B. Gupta https://orcid.org/0000-0002-4385-0799
Mariappan Parans Paranthaman https://orcid.org/0000-0003-3009-8531

References

1. C. X. Tian, F. Lin, and M. M. Doeff, *Acc. Chem. Res.*, **51**, 89 (2018).
2. Q. W. Ran et al., *Acs Appl. Mater. Iterphases*, **12**, 9268 (2020).
3. H. Y. Zhao, Y. F. Nie, Y. F. Li, T. T. Wu, E. Q. Zhao, J. X. Song, and S. Komarneni, *Ceram. Int.*, **45**, 17183 (2019).
4. H. Y. Zhao, F. Li, X. H. Shu, J. T. Liu, T. T. Wu, Z. K. Wang, Y. F. Li, and J. X. Su, *Ceram. Int.*, **44**, 20575 (2018).
5. Z. L. Yu, X. Y. Qu, T. Wan, A. C. Dou, Y. Zhou, X. Q. Peng, M. R. Su, Y. J. Liu, and D. W. Chu, *Acs Appl. Mater. Iterphases*, **12**, 40393 (2020).
6. L. J. Li et al., *Acs Appl. Mater. Iterphases*, **13**, 42554 (2021).
7. K. Zaghib, A. Mauger, H. Groult, J. B. Goodenough, and C. M. Julien, *Materials*, **6**, 1028 (2013).
8. J. Li, L. E. Downie, L. Ma, W. Qiu, and J. R. Dahn, *J. Electrochem. Soc.*, **162**, A1401 (2015).
9. Q. Huang, L. Ma, A. Liu, X. W. Ma, J. Li, J. Wang, and J. R. Dahn, *J. Power Sources*, **390**, 78 (2018).
10. J. B. Goodenough and Y. Kim, *Chem. Mater.*, **22**, 587 (2010).
11. H. Kim, M. G. Kim, H. Y. Jeong, H. Nam, and J. Cho, *Nano Lett.*, **15**, 2111 (2015).
12. F. Lin, I. M. Markus, D. Nordlund, T. C. Weng, M. D. Asta, H. L. L. Xin, and M. M. Doeff, *Nat. Commun.*, **5**, 3529 (2014).
13. K. W. Nam, S. M. Bak, E. Y. Hu, X. Q. Yu, Y. N. Zhou, X. J. Wang, L. J. Wu, Y. M. Zhu, K. Y. Chung, and X. Q. Yang, *Adv. Funct. Mater.*, **23**, 1047 (2013).
14. F. X. Xin, H. Zhou, J. M. Bai, F. Wang, and M. S. Whittingham, *J. Phys. Chem. Lett.*, **12**, 7908 (2021).
15. Q. Q. Zhang, K. Liu, C. Li, S. S. Tan, L. Li, X. G. Sun, W. Li, X. J. Liu, J. L. Zhang, and S. Dai, *Nano Energy*, **86**, 106096 (2021).
16. Y. Cho, P. Oh, and J. Cho, *Nano Lett.*, **13**, 1145 (2013).
17. J. Xiao, N. A. Chernova, and M. S. Whittingham, *Chem. Mater.*, **20**, 7454 (2008).
18. Q. Y. Dong et al., *ACS Appl. Energy Mater.*, **3**, 695 (2020).
19. W. T. Song, J. Harlow, E. Logan, H. Hebecker, M. Coon, L. Molino, M. Johnson, J. Dahn, and M. Metzger, *J. Electrochem. Soc.*, **168**, 090503 (2021).
20. K. Beltrop et al., *Chem. Mater.*, **30**, 2726 (2018).
21. H. Lyu, Y. C. Li, C. J. Jafta, C. A. Bridges, H. M. Meyer, A. Borisevich, M. P. Paranthaman, S. Dai, and X. G. Sun, *J. Power Sources*, **412**, 527 (2019).
22. J. Xie et al., *Acs Nano*, **11**, 7019 (2017).
23. B. H. Han, B. Key, S. H. Lapidus, J. C. Garcia, H. Iddir, J. T. Vaughey, and F. Dogan, *Acs Appl. Mater. Iterphases*, **9**, 41291 (2017).
24. F. Schipper et al., *Adv. Energy Mater.*, **8**, 1701682 (2018).
25. Y. J. Bi et al., *Energy Stor. Mater.*, **24**, 291 (2020).
26. P. Oh, B. H. Song, W. D. Li, and A. Manthiram, *J. Mater. Chem. A*, **4**, 5839 (2016).
27. S. Shrestha, J. Kim, J. Jeong, H. J. Lee, S. C. Kim, H. J. Hah, K. Oh, and S. H. Lee, *J. Electrochem. Soc.*, **168**, 060537 (2021).
28. J. N. Liang et al., *Nano Energy*, **78**, 105107 (2020).
29. X. Li, K. J. Zhang, M. S. Wang, Y. Liu, M. Z. Qu, W. G. Zhao, and J. M. Zheng, *Sustain. Energy Fuels*, **2**, 413 (2018).
30. X. Y. Qu et al., *Nano Energy*, **91**, 106665 (2022).
31. X. Y. Zhang et al., *ACS Appl. Energy Mater.*, **4**, 8641 (2021).
32. H. P. Yang et al., *Adv. Funct. Mater.*, **29**, 1808825 (2019).
33. U. H. Kim et al., *Energy Environ. Sci.*, **11**, 1271 (2018).
34. C. Pouillerie, L. Croguennec, and C. Delmas, *Solid State Ionics*, **132**, 15 (2000).
35. Y. Gao, J. Park, and X. H. Liang, *ACS Appl. Energy Mater.*, **3**, 8978 (2020).
36. N. Phattharasupakun, J. Wutthiprom, S. Duangdangchote, S. Sarawutanukul, C. Tomon, F. Duriyasart, S. Tubtimkuna, C. Aphirakaramwong, and M. Sawangphruk, *Energy Stor. Mater.*, **36**, 485 (2021).
37. X. H. Xiong, D. Ding, Y. F. Bu, Z. X. Wang, B. Huang, H. J. Guo, and X. H. Li, *J. Mater. Chem. A*, **2**, 11691 (2014).
38. S. S. Zhang, X. L. Fan, and C. S. Wang, *Chemelectrochem*, **6**, 1536 (2019).
39. S. Uchida, U. Imamura, and M. Ishikawa, *Electrochem.*, **86**, 29 (2018).
40. J. H. Huang and A. F. Hollenkamp, *J. Phys. Chem. C*, **114**, 21840 (2010).
41. C. J. Jafta et al., *Adv. Funct. Mater.*, **31**, 2008708 (2021).
42. D. H. Cho, C. H. Jo, W. Cho, Y. J. Kim, H. Yashiro, Y. K. Sun, and S. T. Myung, *J. Electrochem. Soc.*, **161**, A920 (2014).
43. C. J. Jafta, K. I. Ozoemena, M. K. Mathe, and W. D. Roos, *Electrochim. Acta*, **85**, 411 (2012).
44. X. Y. Zhang, W. J. Jiang, A. Mauger, Qilu, F. Gendron, and C. M. Julien, *J. Power Sources*, **195**, 1292 (2010).
45. E. D. Orlova, A. A. Savina, S. A. Abakumov, A. V. Morozov, and A. M. Abakumov, *Symmetry-Basel*, **13**, 1628 (2021).
46. H. J. Noh, S. Youn, C. S. Yoon, and Y. K. Sun, *J. Power Sources*, **233**, 121 (2013).
47. B. Philippe, R. Dedryvere, M. Gorgoi, H. Rensmo, D. Gonbeau, and K. Edstrom, *J. Am. Chem. Soc.*, **135**, 9829 (2013).
48. J. Wang, J. Yang, Q. B. Xiao, L. J. Jia, H. Z. Lin, and Y. G. Zhang, *Acs Appl. Mater. Iterphases*, **11**, 30500 (2019).
49. D. Parikh, L. X. Geng, H. L. Lyu, C. J. Jafta, H. S. Liu, H. M. Meyer III, J. H. Chen, X.-G. Sun, S. Dai, and J. L. Li, *Acs Appl. Mater. Iterphases*, **13**, 55145 (2021).
50. R. Jung, M. Metzger, F. Maglia, C. Stinner, and H. A. Gasteiger, *J. Electrochem. Soc.*, **164**, A1361 (2017).
51. M. Stich, M. Gottlinger, M. Kurniawan, U. Schmidt, and A. Bund, *J. Phys. Chem. C*, **122**, 8836 (2018).
52. S. Solchenbach, M. Metzger, M. Egawa, H. Beyer, and H. A. Gasteiger, *J. Electrochem. Soc.*, **165**, A3022 (2018).
53. X. G. Sun and C. A. Angell, *Electrochem. Commun.*, **11**, 1418 (2009).